Coarse Graining DNA: Symmetry, Nonlocal Elasticity, and Persistence Length

Yair Augusto Gutiérrez Fosado,[1,*] Fabio Landuzzi,[2,*] and Takahiro Sakaue[3,†]
[1]School of Physics and Astronomy, University of Edinburgh, Peter Guthrie Tait Road, Edinburgh, EH9 3FD, United Kingdom
[2]Centro CMP3VdA, Istituto Italiano di Tecnologia, via Lavoratori Vittime del Col du Mont 28, 11100, Aosta, Italy
[3]Department of Physics and Mathematics, Aoyama Gakuin University,
5-10-1 Fuchinobe, Chuo-ku, Sagamihara-shi, Kanagawa 252-5258, Japan

(Received 3 June 2022; accepted 6 January 2023; published 3 February 2023)

While the behavior of double-stranded DNA at mesoscopic scales is fairly well understood, less is known about its relation to the rich mechanical properties in the base-pair scale, which is crucial, for instance, to understand DNA-protein interactions and the nucleosome diffusion mechanism. Here, by employing the rigid base-pair model, we connect its microscopic parameters to the persistence length. Combined with all-atom molecular dynamic simulations, our scheme identifies relevant couplings between different degrees of freedom at each coarse-graining step. This allows us to clarify how the scale dependence of the elastic moduli is determined in a systematic way encompassing the role of previously unnoticed off-site couplings between deformations with different parity.

DOI: 10.1103/PhysRevLett.130.058402

The mechanical properties of DNA play a vital role in fundamental biological processes [1–3]. Because of its hierarchical structure, the behavior of DNA depends on the length scales, and so does the model to describe it. At mesoscopic length scales, DNA exhibits an entropic elasticity, for which one can employ a generic flexible polymer (FP) model [4]. On the scale of 50–100 nm, the bending and twisting elastic degrees of freedom become apparent, and DNA is described by the wormlike chain (WLC) model [5,6]. However, understanding the mechanical behavior of DNA at even shorter length scales, relevant to, e.g., DNA-protein interactions, requires a more detailed description that accounts for structural features of DNA and sequence specificity. The standard model for that purpose is the rigid base-pair (RBP) model, in which a DNA molecule is described as a succession of rigid subunits representing base pairs [7,8].

What is the relation between FP, WLC, and RBP models? To answer this question, a suitable strategy is to leave the sequence-specific effect aside and adopt an average base-pair description. Recall that the mechanical behavior of DNA at the mesoscopic scale probed by single-molecule experiments is arguably one of the most successful topics studied in biophysics to date [5,9–17]. In typical experiments, the extension of a DNA molecule several tens kbp long, was measured as a function of an applied force and/or torque [5,9–13]. This provided a rigorous test to existing theories based on FP and WLC and led to the determination of the bending (l_b) and torsional (l_t) persistence lengths [14–17]. More recently, however, experiments have reported the high flexibility of short DNA fragments characterized by a shorter effective l_b, whose origin and relation to the mesoscopic models have been under active debate [18–22]. In this Letter, we address this aspect by a combination of theory and all-atom simulations of DNA (performed at $[\mathrm{NaCl}] = 150$ mM; see details in Ref. [23]) that help us to elucidate the relation between models of DNA elasticity at different scales.

In principle, a large number of parameters in the RBP model can be evaluated through the analysis of DNA structural fluctuation obtained from all-atom simulations or high-resolution crystal structural data. Past studies have often adopted the local free energy assumption to simplify the RBP model and attempted to relate its parameters to persistence lengths [7,28–30]. However, such an assumption is not generally correct [8,31,32], which implies that the deformation of DNA is length-scale dependent. Here, in order to elaborate on the nonlocal nature of the RBP model, we present a systematic coarse-graining scheme from RBP to FP through an intermediate model, which we call the generalized wormlike chain (GWLC) model (Fig. 1). This pinpoints the role of couplings between different degrees of freedom at each coarse-graining step. Our main results are (i) the formulas for the persistence lengths in terms of the RBP model parameters in the long-wavelength limit, which are in good agreement with known values, and (ii) a quantification of the scale-dependent DNA elasticity, which is compatible with the high flexibility of short DNA fragments [18–21]. Of crucial importance for our discussion is the symmetry argument based on the molecular structure of the DNA double helix [6]. This restricts the form of the free energy, and, hence, it classifies the coupling terms as either symmetric or antisymmetric. The latter, although largely neglected in the literature, produces off-site correlations between deformation degrees of freedom with opposite

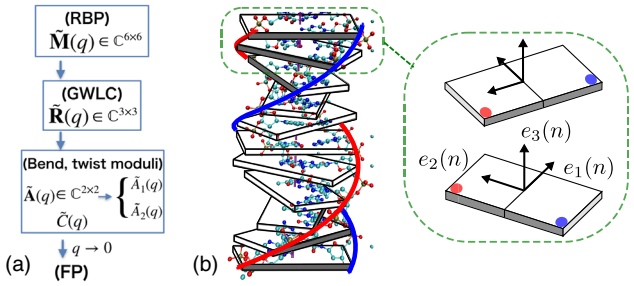

FIG. 1. (a) Coarse-graining scheme from RBP model to FP model of DNA. RBP and GWLC models are characterized by the wave number (q)-dependent stiffness matrix $\tilde{\mathbf{M}}(q) \in \mathbb{C}^{6\times6}$ and $\tilde{\mathbf{R}}(q) \in \mathbb{C}^{3\times3}$, respectively. From the latter, q-dependent bend and twist moduli are extracted. The $q \to 0$ limit leads to the persistence lengths characterizing the FP model. (b) Definition of the orthonormal frame in the RBP model. Starting from the center of the nth brick, $\boldsymbol{e}_3(n)$ points to that of the $n+1$th brick, and $\boldsymbol{e}_1(n)$ lies in the nth brick and points to the major groove direction, which then determine $\boldsymbol{e}_2(n) = \boldsymbol{e}_3(n) \times \boldsymbol{e}_1(n)$.

parity and affects the DNA flexibility on the scale of several base pairs.

In the RBP model, DNA is described as a succession of rigid subunits representing base pairs, which are numbered by the index $n \in [-N/2, N/2)$ starting from one end of the DNA chain, where N (assumed to be even) is the total number of base-pair steps. The position $\boldsymbol{r}(n)$ of the nth base pair and its orientation, described by an embedded orthonormal frame $[\boldsymbol{e}_1(n), \boldsymbol{e}_2(n), \boldsymbol{e}_3(n)]$, determine the DNA configuration (Fig. 1). To describe the local deformation of a DNA molecule, one identifies a vector $\boldsymbol{\Omega}(n) \in \mathbb{R}^6$ from the relative position and orientation between consecutive base pairs (n and $n+1$), such that it maps the former to the latter [33,34]. The first three components $\boldsymbol{\Omega}_r(n) \equiv [\Omega_1(n), \Omega_2(n), \Omega_3(n)]$ represent the rotational angles per unit length, commonly referred as tilt, roll, and twist. Similarly, the last three components $\boldsymbol{\Omega}_t(n) \equiv [\Omega_4(n), \Omega_5(n), \Omega_6(n)]$ represent the translational displacements per unit length, commonly referred as shift, slide, and rise. The free energy takes the quadratic form

$$E[\{\delta\boldsymbol{\Omega}(n)\}] = \frac{a}{2}\sum_{n'}\sum_{n} \delta\boldsymbol{\Omega}^T(n')\mathbf{M}(n',n)\delta\boldsymbol{\Omega}(n), \qquad (1)$$

where sums run over all possible pairs of base-pair steps, a ($= 0.34$ nm) is the average distance between consecutive base pairs, and $\delta\boldsymbol{\Omega}(n) = \boldsymbol{\Omega}(n) - \langle\boldsymbol{\Omega}(n)\rangle$ represents the deviation from the thermal average $\langle\boldsymbol{\Omega}(n)\rangle$. The stiffness matrix $\mathbf{M}(n,m) \in \mathbb{R}^{6\times6}$ is positive definite and encodes for all the interactions (including electrostatics) between deformations at base-pair steps n and m. Some remarks on the M matrix are as follows.

(i) *Reversal and translational invariance for average sequence.*—Since we are interested in the average base-pair description, Eq. (1) can be rewritten as

$$E[\{\delta\boldsymbol{\Omega}(n)\}] = \frac{a}{2}\sum_{n}\sum_{m} \delta\boldsymbol{\Omega}^T(n+m)\mathbf{M}(m)\delta\boldsymbol{\Omega}(n), \qquad (2)$$

where $\boldsymbol{M}$ depends on the separation $m = |n' - n|$ between base pairs [31]. Introducing the Fourier transform as

$$\delta\tilde{\boldsymbol{\Omega}}(q) = \sum_{n=-N/2}^{N/2-1} \delta\boldsymbol{\Omega}(n)e^{-2\pi iqn/N}, \qquad (3)$$

with the integer $q \in -[N/2, N/2)$, the energy function (2) is represented as a sum over independent mode contributions:

$$E[\{\delta\tilde{\boldsymbol{\Omega}}(q)\}] = \frac{a}{2N}\sum_{q} \delta\tilde{\boldsymbol{\Omega}}^T(q)\tilde{\mathbf{M}}(q)\delta\tilde{\boldsymbol{\Omega}}(-q). \qquad (4)$$

(ii) *Local approximation is not valid.*—From the equipartition theorem, we find

$$\langle\delta\tilde{\boldsymbol{\Omega}}(q)\delta\tilde{\boldsymbol{\Omega}}^T(-q)\rangle = \frac{Nk_BT}{a}\tilde{\mathbf{M}}^{-1}(q). \qquad (5)$$

If one neglects correlations between deformations at different base pairs, any component of $\langle\delta\tilde{\boldsymbol{\Omega}}(q)\delta\tilde{\boldsymbol{\Omega}}^T(-q)\rangle$ just exhibits a white power spectrum; hence, the stiffness matrix takes a local form $\mathbf{M}(m) = \mathbf{M}^o\delta_{m0}$, making Eq. (2) a simple elastic free energy. However, our numerical simulations (Fig. 2) show a colored power spectrum; hence, distal correlations exist in the RBP model of DNA [31,32]. The characteristic bell-shape spectra can be fitted by a Lorentzian, indicating an exponentially decaying memory along DNA [23], which leads to the softer mechanical behavior in short length scales. The slide degree of freedom (M_{55}) is against this trend exhibiting nonmonotonic q dependence. Note also that among the translational degrees of freedom the rise (M_{66}) is very stiff, while the shift (M_{44}) and the slide are soft. We shall see below that these features make the coupling of the rotational degrees of freedom with the shift and the slide important to determine the mechanical parameters in GWLC.

(iii) *Conditions imposed by symmetry argument.*—Marko and Siggia predicted the coupling between bend (roll) and twist based on the symmetry argument of the DNA double helix [6], effects of which have been studied in several contexts, including the structure of nucleosomal DNA [35,36] and the torque response in experiments [17]. Here, we generalize this argument (see also Ref. [31]). Under the reversal of contour coordinate $n \to \hat{n} \equiv -n$, the deformation vector is transformed as $\Omega_i(n) \to \hat{\Omega}_i(\hat{n}) = \epsilon_i\Omega_i(n)$, where $\epsilon_1 = \epsilon_4 = -1$ and $\epsilon_2 = \epsilon_3 = \epsilon_5 = \epsilon_6 = 1$; i.e., tilt and shift are odd, and other deformations are even

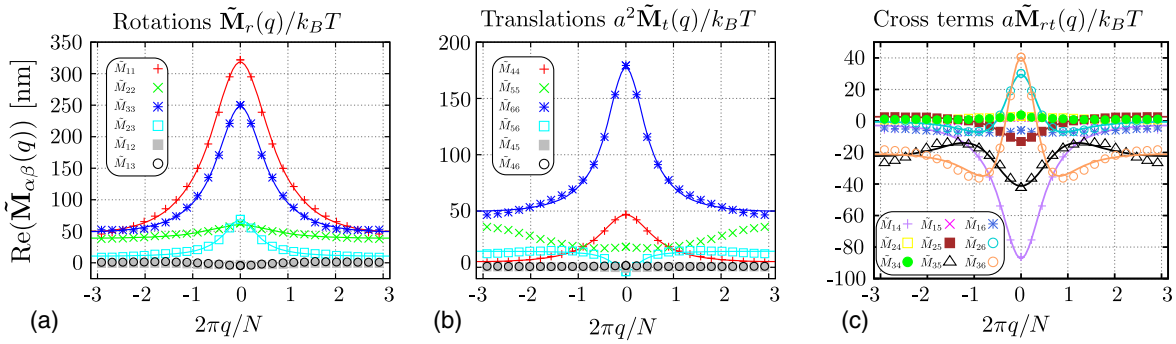

FIG. 2. Real part of $\tilde{\mathbf{M}}(q)$ numerically evaluated using Eq. (5) represented in units of length. Lines are fit functions, where we assume exponential correlations along DNA [23]. From left to right, plots show the components of $\tilde{\mathbf{M}}_r(q)/k_BT$, $a^2\tilde{\mathbf{M}}_t(q)/k_BT$, and $a\tilde{\mathbf{M}}_{rt}(q)/k_BT$, which correspond to rotational, translational, and coupling submatrices, respectively (k_BT is the thermal energy). Note that some components $(M_{12}, M_{13}, M_{45}, M_{46}, M_{24}, M_{34}, M_{15}, M_{16})$ have a negligible real part and instead exhibit characteristic antisymmetric profiles in their imaginary part [23].

under the reversal operation [8,23,31]. Since the free energy is invariant under this operation, $M_{\alpha\beta}(m) = \epsilon_\alpha\epsilon_\beta M_{\alpha\beta}(-m) = \epsilon_\alpha\epsilon_\beta M_{\beta\alpha}(m)$. In Fourier space, the components of the stiffness matrix with the index pair of the same parity (i.e., $\epsilon_\alpha\epsilon_\beta = 1$) are real $\tilde{M}_{\alpha\beta}(q) = |\tilde{M}_{\alpha\beta}(q)|$, even functions of q and constitute the symmetric part of $\tilde{M}(q)$; i.e., $\tilde{M}_{\alpha\beta}(q) = \tilde{M}_{\beta\alpha}(q) = \tilde{M}_{\alpha\beta}(-q)$. On the other hand, the components with the index pair of the different parity (i.e., $\epsilon_\alpha\epsilon_\beta = -1$) are imaginary $\tilde{M}_{\alpha\beta}(q) = i|\tilde{M}_{\alpha\beta}(q)|$, odd functions of q and constitute the antisymmetric part of $\tilde{M}(q)$; i.e., $\tilde{M}_{\alpha\beta}(q) = -\tilde{M}_{\beta\alpha}(q) = -\tilde{M}_{\alpha\beta}(-q)$. The last condition implies the antisymmetric components vanish in the $q \to 0$ limit. The results from all-atom simulation are all consistent with this symmetry argument; see Fig. 2 [23].

(iv) *Decomposition into rotational and translational components.*—In line with the decomposition of the deformation vector $\mathbf{\Omega}(n) = [\mathbf{\Omega}_r(n), \mathbf{\Omega}_t(n)]$, one can decompose $\mathbf{M}(m)$ as

$$\mathbf{M}(m) = \begin{pmatrix} \mathbf{M}_r(m) & \mathbf{M}_{rt}(m) \\ \mathbf{M}_{tr}(m) & \mathbf{M}_t(m) \end{pmatrix}, \tag{6}$$

where the submatrices $\mathbf{M}_r(m), \mathbf{M}_t(m) \in \mathbb{R}^{3\times3}$ encode the stiffness of the RBP model of DNA for the rotational and translational deformations, respectively, and the submatrices $\mathbf{M}_{rt}(m), \mathbf{M}_{tr}(m) \in \mathbb{R}^{3\times3}$ represent the rotational-translational coupling with $[M_{tr}(m)]_{\alpha\beta} = \epsilon_\alpha\epsilon_\beta[M_{rt}(m)]_{\beta\alpha}$.

In the first step of the coarse graining, we integrate out the translational degrees of freedom $\mathbf{\Omega}_t(n)$. Exploiting the Gaussian nature of the energy function (4), one finds the energy function of the GWLC [31]:

$$E_r[\{\delta\tilde{\mathbf{\Omega}}_r(q)\}] = \frac{a}{2N}\sum_q \delta\tilde{\mathbf{\Omega}}_r^T(q)\tilde{\mathbf{R}}(q)\delta\tilde{\mathbf{\Omega}}_r(-q), \tag{7}$$

which depends only on the rotational degrees of freedom $\mathbf{\Omega}_r(n)$. The corresponding stiffness matrix $\mathbf{R}(m) \in \mathbb{R}^{3\times3}$ is obtained from $\mathbf{M}(m) \in \mathbb{R}^{6\times6}$ as

$$\tilde{\mathbf{R}}(q) = \tilde{\mathbf{M}}_r(q) - \tilde{\mathbf{M}}_{rt}(q)\tilde{\mathbf{M}}_t^{-1}(q)\tilde{\mathbf{M}}_{tr}(q), \tag{8}$$

which is known as the Schur complement of $\tilde{\mathbf{M}}_t(q)$ in $\tilde{\mathbf{M}}(q)$ [37].

For conciseness, we introduce the following expression relating the components of two matrices:

$$\tilde{R}_{\alpha\beta}(q) = [\tilde{M}_{\alpha\beta}(q)]^{(4,5,6)}, \qquad \alpha,\beta \in (1,2,3), \tag{9}$$

where we introduce the contraction operation

$$[M_{\alpha\beta}]^{(\delta)} \equiv M_{\alpha\beta} - \frac{M_{\alpha\delta}M_{\delta\beta}}{M_{\delta\delta}} \tag{10}$$

on the component of an arbitrary matrix $M_{\alpha\beta}$ with the integrated degrees of freedom indicated by the superscript $\delta(\neq\alpha,\beta)$. By applying the contraction operation sequentially, one can readily define the double contraction

$$[M_{\alpha\beta}]^{(\delta,\gamma)} = [[M_{\alpha\beta}]^{(\delta)}]^{(\gamma)} = [[M_{\alpha\beta}]^{(\gamma)}]^{(\delta)}, \tag{11}$$

which embodies the effect of integrating two degrees of freedom $\delta,\gamma(\neq\alpha,\beta)$ out simultaneously. The order of the contraction is irrelevant, and the generalization to multiple contractions integrating more than two degrees of freedom is straightforward.

The same symmetry argument as for $\mathbf{M}$ applies to $\mathbf{R}$ [23]. The antisymmetric components $\tilde{R}_{12}(q)$ and $\tilde{R}_{13}(q)$ are purely imaginary and odd functions of q, while the rest are symmetric and real, even functions of q; see Figs. 3 and S4 [23]. While the characteristic q dependence of $\tilde{R}_{\alpha\beta}$ is similar to that of corresponding $\tilde{M}_{r\alpha\beta}$, the magnitude is reduced upon coarse graining. Indeed, our contraction

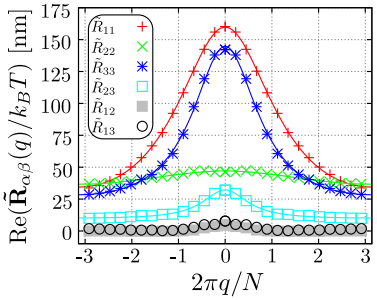

FIG. 3. Real part of $\tilde{\mathbf{R}}(q)$ (GWLC model), obtained through contraction operation [Eq. (8)] applied to $\tilde{\mathbf{M}}(q)$. Lines are fit functions with exponential memory along DNA [23]. $\tilde{R}_{12}(q)$ and $\tilde{R}_{13}(q)$ have a negligible real part and exhibit antisymmetric characteristic profiles in their imaginary part [23].

formula (10) predicts the decrease in the effective rotational stiffness, where the degree of reduction is controlled by the stiffness of the integrated degrees of freedom and the coupling strength with it. We observe that, while the stiffness of the tilt and the twist decreases roughly by half, that of the roll is rather insensitive. This is understood from the negligibly weak roll-slide coupling ($\tilde{M}_{25}$) compared to tilt-shift ($\tilde{M}_{14}$) and twist-slide ($\tilde{M}_{35}$) couplings, whereas the coupling with rise makes only a negligible contribution due to its high stiffness ($\tilde{M}_{66}$). Importantly, our result on the $\tilde{\mathbf{R}}(q)$ is in quantitative agreement with the recent report based on the direct analysis of GWLC [31].

Next, we integrate out the twisting (or bending) degree of freedom $\Omega_3(n)$ [or $\Omega_1(n)$ and $\Omega_2(n)$]. The procedure of this second step of coarse graining $\tilde{\mathbf{R}} \to \tilde{\mathbf{A}}$ (or $\tilde{\mathbf{R}} \to \tilde{C}$) is essentially the same as that of the first step $\tilde{\mathbf{M}} \to \tilde{\mathbf{R}}$ [23]. The Gaussianity of the energy function (7) allows us to construct

$$E_b[\{\delta\tilde{\mathbf{\Omega}}_b(q)\}] = \frac{a}{2N}\sum_q \delta\tilde{\mathbf{\Omega}}_b^T(q)\tilde{\mathbf{A}}(q)\delta\tilde{\mathbf{\Omega}}_b(-q), \quad (12)$$

which depends only on the bending degrees of freedom $\mathbf{\Omega}_b(n) = [\Omega_1(n), \Omega_2(n)]$, where the bending stiffness matrix $\mathbf{A}(m) \in \mathbb{R}^{2\times 2}$ is antisymmetric with Fourier transform displaying imaginary off-diagonal elements; i.e., $\tilde{A}_{12}(q) = -\tilde{A}_{12}(-q) = -\tilde{A}_{21}(q)$ as obtained from the rotational stiffness matrix $\mathbf{R}(m) \in \mathbb{R}^{3\times 3}$:

$$\tilde{A}_{\alpha\beta}(q) = [\tilde{R}_{\alpha\beta}(q)]^{(3)}, \qquad \alpha,\beta \in (1,2). \quad (13)$$

Finally, one can disentangle tilt and roll as $\tilde{A}_1(q) = [\tilde{A}_{11}(q)]^{(2)}$ and $\tilde{A}_2(q) = [\tilde{A}_{22}(q)]^{(1)}$ (see Fig. 4). Similarly, one can construct the coarse-grained twist energy function

$$E_t[\{\delta\tilde{\Omega}_3(q)\}] = \frac{a}{2N}\sum_q \delta\tilde{\Omega}_3^T(q)\tilde{C}(q)\delta\tilde{\Omega}_3(-q), \quad (14)$$

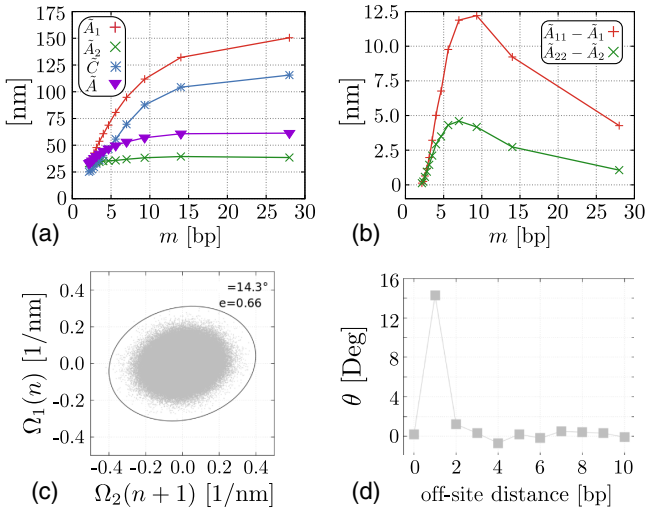

FIG. 4. (a) Scale-dependent bend (tilt and roll) and twist moduli $\tilde{A}_1(q)$, $\tilde{A}_2(q)$, and $\tilde{C}(q)$ as a function of the base-pair separation $m = N/q$. $\tilde{A}(q)$ is the harmonic mean of tilt and roll. (b) Softening of the tilt $\tilde{A}_{11}(q) - \tilde{A}_1(q)$ and the roll $\tilde{A}_{22}(q) - \tilde{A}_2(q)$ at finite $q \neq 0$ due to the tilt-roll coupling. (c) Scatter plot of the off-site correlation $\delta\Omega_1(n)$ and $\delta\Omega_2(n+m)$ with $m = 1$. The 95% confidence ellipse is shown. The tile angle that the ellipse makes with the x axis is θ and its eccentricity e. (d) θ as a function of the off-site distance m.

which depends only on the twisting degrees of freedom $\Omega_3(n)$ with the stiffness $\tilde{C}(q)$ given by

$$\tilde{C}(q) = [\tilde{R}_{33}(q)]^{(1,2)}. \quad (15)$$

In the long-wavelength limit ($q \to 0$), all the antisymmetric components in the stiffness matrix vanish [23]. Equations (13) and (15) then lead to

$$\tilde{A}_1(0) = \tilde{R}_{11}(0), \qquad \tilde{A}_2(0) = \tilde{R}_{22}(0) - \frac{\tilde{R}_{23}(0)^2}{\tilde{R}_{33}(0)} \quad (16)$$

and the twist modulus

$$\tilde{C}(0) = \tilde{R}_{33}(0) - \frac{\tilde{R}_{23}(0)^2}{\tilde{R}_{22}(0)}. \quad (17)$$

These effective moduli evaluated at $q \to 0$ govern the large-scale bending and twisting behaviors of DNA, leading to the persistence lengths

$$l_b = \frac{2}{k_BT}\frac{\tilde{A}_1(0)\tilde{A}_2(0)}{[\tilde{A}_1(0) + \tilde{A}_2(0)]} \quad \text{and} \quad l_t = \frac{2\tilde{C}(0)}{k_BT}. \quad (18)$$

Equations (16)–(18) together with Eq. (9) provide a quantitative connection between the RBP model and the WLC and FP models of DNA (see Ref. [23] for the explicit

formula). From the RBP parameters $\tilde{\mathbf{M}}(0)$ (Fig. 2), our formula leads to $\tilde{A}_1(0)/k_BT = 156$ nm, $\tilde{A}_2(0)/k_BT = 39$ nm, thus $l_b = 62$ nm, and $\tilde{C}(0)/k_BT = l_t/2 = 120$ nm, both of which agree with coarse-grained simulations [38], all-atom simulations [31], and experiments [11,17]. Our construction reveals that, in addition to the softened roll and twist due to their coupling [31,39] [see Eqs. (16) and (17)], a similar softening mechanism is at work in the coarse-graining step from the RBP to the GWLC model, where the tilt-shift and twist-slide couplings play a decisive role to determine the renormalized stiffness matrix $\tilde{\mathbf{R}}$; see Eq. (9).

Recent experiments have reported that short DNA fragments exhibit much higher flexibility than expected from its "bulk" elastic property measured in, e.g., single-molecule experiments [18–21]. In accord with it, the bend and twist moduli as functions of the length scale $m = N/q$ clearly show softer behavior on a small length scale [Fig. 4(a)]. It is worth noting here that the antisymmetric part of the stiffness matrix is generally nonvanishing at finite $q \neq 0$. Although smaller in magnitude than that of its symmetric counterpart (Figs. S2, S4, and S5 [23]), its effect is non-negligible for the quantitative account for the high flexibility on a small scale. Therefore, one needs to take this intrinsic property of double-stranded DNA into account on top of the often invoked kinks [18–20] or local denaturation bubbles [22] as a softening mechanism. As an example, Fig. 4(b) shows the softening of the bending response due to the antisymmetric tilt-roll coupling. This is mirrored in the off-site correlation between the tilt and the roll [Figs. 4(c) and 4(d)].

The nonlocal elasticity naturally arises upon coarse graining, as demonstrated for a mechanical toy model with internal degrees of freedom [32]. A simple (structureless) polyelectrolyte shares this common feature, where the electrostatic effect with counter ions and salts is renormalized to the effective bending rigidity [40,41]. For DNA, both the internal (double-helix) structure and the electrostatic effect contribute to the nonlocal elasticity. The fact that the correlation length ξ in the stiffness matrices is on the order of the Debye length (Tables S1–S4) indicates that the electrostatic effect grows and dominates in lower salt conditions.

In conclusion, we have provided a quantitative connection between models of DNA in different spatial resolution, from the base-pair to mesoscopic scales. We expect that the scale-dependent mechanics of DNA is indispensable for the quantitative understanding of DNA-protein interactions, which often induce the tight bend and twist on the scale of several base pairs. Such features are seen, for instance, in nucleosomes, dictating its structural fluctuation and dynamics [35]. Also relevant is the DNA response to the intercalators and groove binders, the understanding of which is important for better design of anticancer drugs [42]. Further studies are awaited, which need to address the sequence effect, too.

We thank E. Carlon for stimulating discussions. T. S. is supported by JSPS KAKENHI (No. JP18H05529 and No. JP21H05759) from MEXT, Japan.

*These authors contributed equally to this work.
†Corresponding author.
sakaue@phys.aoyama.ac.jp

[1] H. G. Garcia, P. Grayson, L. Han, M. Inamdar, J. Kondev, P. C. Nelson, R. Phillips, J. Widom, and P. A. Wiggins, Biological consequences of tightly bent DNA: The other life of a macromolecular celebrity, Biopolymers **85**, 115 (2007).
[2] A. Aggarwal, S. Naskar, A. K. Sahoo, S. Mogurampelly, A. Garai, and P. K. Maiti, What do we know about DNA mechanics so far?, Curr. Opin. Struct. Biol. **64**, 42 (2020).
[3] P. C. Nelson, Spare the (elastic) rod, Science **337**, 1045 (2012).
[4] P.-G. de Gennes, *Scaling Concepts in Polymer Physics* (Cornell University Press, Ithaca, NY, 1979).
[5] C. Bustamante, J. F. Marko, E. D. Siggia, and S. Smith, Entropic elasticity of λ-phage DNA, Science **265**, 1599 (1994).
[6] J. F. Marko and E. D. Siggia, Bending and twisting elasticity of DNA, Macromolecules **27**, 981 (1994).
[7] W. K. Olson, A. A. Gorin, X.-J. Lu, L. M. Hock, and V. B. Zhurkin, DNA sequence-dependent deformability deduced from protein–DNA crystal complexes, Proc. Natl. Acad. Sci. U.S.A. **95**, 11163 (1998).
[8] F. Lankaš, O. Gonzalez, L. M. Heffler, G. Stoll, M. Moakher, and J. H. Maddocks, On the parameterization of rigid base and basepair models of DNA from molecular dynamics simulations, Phys. Chem. Chem. Phys. **11**, 10565 (2009).
[9] T. T. Perkins, D. E. Smith, R. G. Larson, and S. Chu, Stretching of a single tethered polymer in a uniform flow, Science **268**, 83 (1995).
[10] C. Bustamante, Z. Bryant, and S. B. Smith, Ten years of tension: single-molecule DNA mechanics, Nature (London) **421**, 423 (2003).
[11] J. Lipfert, J. W. J. Kerssemakers, T. Jager, and N. H. DekkerMagnetic torque tweezers: measuring torsional stiffness in DNA and RecA-DNA filaments, Nat. Methods **7**, 977 (2010).
[12] J. Lipfert, M. Wiggin, J. W. J. Kerssemakers, F. Pedaci, and N. H. Dekker, Freely orbiting magnetic tweezers to directly monitor changes in the twist of nucleic acids, Nat. Commun. **2**, 439 (2011).
[13] X. J. A. Janssen, J. Lipfert, T. Jager, R. Daudey, J. Beekman, and N. H. Dekker, Electromagnetic torque tweezers: A versatile approach for measurement of single-molecule twist and torque, Nano Lett. **12**, 3634 (2012).
[14] J. F. Marko and E. D. Siggia, Stretching DNA, Macromolecules **28**, 8759 (1995).
[15] T. Odijk, Stiff chains and filaments under tension, Macromolecules **28**, 7016 (1995).
[16] J. D. Moroz and P. Nelson, Entropic elasticity of twist-storing polymers, Macromolecules **31**, 6333 (1998).

[17] S. K. Nomidis, F. Kriegel, W. Vanderlinden, J. Lipfert, and E. Carlon, Twist-Bend Coupling and the Torsional Response of Double-Stranded DNA, Phys. Rev. Lett. **118**, 217801 (2017).
[18] T. Schindler, A. González, R. Boopathi, M. M. Roda, L. Romero-Santacreu, A. Wildes, L. Porcar, A. Martel, N. Theodorakopoulos, S. Cuesta-López, D. Angelov, T. Unruh, and M. Peyrard, Kinky DNA in solution: Small-angle-scattering study of a nucleosome positioning sequence, Phys. Rev. E **98**, 042417 (2018).
[19] C. Yuan, H. Chen, X. W. Lou, and L. A. Archer, DNA Bending Stiffness on Small Length Scales, Phys. Rev. Lett. **100**, 018102 (2008).
[20] P. A. Wiggins, T. van der Heijden, F. Moreno-Herrero, A. Spakowitz, R. Phillips, J. Widom, C. Dekker, and P. C. Nelson, High flexibility of DNA on short length scales probed by atomic force microscopy, Nat. Nanotechnol. **1**, 137 (2006).
[21] A. Noy and R. Golestanian, Length Scale Dependence of DNA Mechanical Properties, Phys. Rev. Lett. **109**, 228101 (2012).
[22] N. Destainville, M. Manghi, and J. Palmeri, Microscopic mechanism for experimentally observed anomalous elasticity of DNA in two dimensions, Biophys. J. **96**, 4464 (2009).
[23] See Supplemental Material at http://link.aps.org/supplemental/10.1103/PhysRevLett.130.058402 for a detailed discussion on the symmetry argument, the coarse-gaining procedure, the explicit formula for the persistence lengths, the functional forms of the scale-dependent elastic moduli, and the method of all-atom MD simulations. Supplemental Material further includes Refs. [24–27].
[24] E. Trifonov, R. Tan, and S. Harvey, in *Static Persistence Length of DNA. Structure and Expression: Proceedings of the Fifth Conversation in the Discipline Biomolecular Stereodynamics*, edited by M. Sarma and R. Sarma (Adenine Press, Schenectady, NY, 1988).
[25] R. Lavery, M. Moakher, J. H. Maddocks, D. Petkeviciute, and K. Zakrzewska, Conformational analysis of nucleic acids revisited: Curves+, Nucl. Acids Res. **37**, 5917 (2009).
[26] D. Van Der Spoel, E. Lindahl, B. Hess, G. Groenhof, A. E. Mark, and H. J. C. Berendsen, GROMACS: Fast, flexible, and free, J. Comput. Chem. **26**, 1701 (2005).
[27] I. Ivani *et al.*, Parmbsc1: A refined force field for DNA simulations, Nat. Methods **13**, 55 (2016).
[28] F. Lankaš, J. Šponer, J. Langowski, and T. E. Cheatham III, DNA basepair step deformability inferred from molecular dynamics simulations, Biophys. J. **85**, 2872 (2003).
[29] N. B. Becker and R. Everaers, From rigid base pairs to semiflexible polymers: Coarse-graining DNA, Phys. Rev. E **76**, 021923 (2007).
[30] A. Pérez, F. Lankas, F. J. Luque, and M. Orozco, Towards a molecular dynamics consensus view of B-DNA flexibility, Nucl. Acids Res. **36**, 2379 (2008).
[31] E. Skoruppa, A. Voorspoels, J. Vreede, and E. Carlon, Length-scale-dependent elasticity in DNA from coarse-grained and all-atom models, Phys. Rev. E **103**, 042408 (2021).
[32] M. Segers, A. Voorspoels, T. Sakaue, and E. Carlon, Mechanical properties of nucleic acids and the non-local twistable wormlike chain model, J. Chem. Phys. **156**, 234105 (2022).
[33] R. Dickerson, Definitions and nomenclature of nucleic acid structure components, Nucl. Acids Res. **17**, 1797 (1989).
[34] W. K. Olson, M. Bansal, S. K. Burley, R. E. Dickerson, M. Gerstein, S. C. Harvey, U. Heinemann, X.-J. Lu, S. Neidle, Z. Shakked, H. Sklenar, M. Suzuki, C.-S. Tung, E. Westhof, C. Wolberger, and H. M. Berman, A standard reference frame for the description of nucleic acid base-pair geometry, J. Mol. Biol. **313**, 229 (2001).
[35] E. Skoruppa, S. K. Nomidis, J. F. Marko, and E. Carlon, Bend-Induced Twist Waves and the Structure of Nucleosomal DN, Phys. Rev. Lett. **121**, 088101 (2018).
[36] F. Mohammad-Rafiee and R. Golestanian, Elastic Correlations in Nucleosomal DNA Structure, Phys. Rev. Lett. **94**, 238102 (2005).
[37] *The Schur Complement and its Applications*, edited by F. Zhang, Numerical Methods and Algorithms (Springer, New York, 2005).
[38] J. S. Mitchell, J. Glowacki, A. E. Grandchamp, R. S. Manning, and J. H. Maddocks, Sequence-Dependent Persistence Lengths of DNA, J. Chem. Theory Comput. **13**, 1539 (2017).
[39] Y. A. Gutiérrez Fosado, F. Landuzzi, and T. Sakaue, Twist dynamics and buckling instability of ring DNA: the effect of groove asymmetry and anisotropic bending, Soft Matter **17**, 1530 (2021).
[40] J.-L. Barrat and J.-F. Joanny, Persistence Length of Polyelectrolyte Chains, Europhys. Lett. **24**, 333 (1993).
[41] J.-L. Barrat and F. Joanny, Theory of polyelectrolyte solutions, in *Advances in Chemical Physics* (John Wiley & Sons, New York, 1996), pp. 1–66, 10.1002/9780470141533.ch1.
[42] A. K. Sahoo, B. Bagchi, and P. K. Maiti, Understanding enhanced mechanical stability of DNA in the presence of intercalated anticancer drug: Implications for DNA associated processes, J. Chem. Phys. **151**, 164902 (2019).